CrossMark

A modified discrete algebraic reconstruction technique for multiple grey image reconstruction for limited angle range tomography

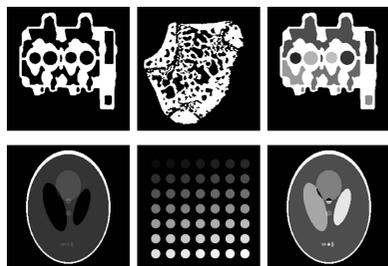**Zhiting Liang, Yong Guan, Gang Liu, Xiangyu Chen, Fahu Li, Pengfei Guo and Yangchao Tian***

National Synchrotron Radiation Laboratory, University of Science and Technology of China, 3#419, No.42 Hezuohua South Road, Hefei, Anhui 230029, People's Republic of China. *Correspondence e-mail: ychtian@ustc.edu.cn

The 'missing wedge', which is due to a restricted rotation range, is a major challenge for quantitative analysis of an object using tomography. With prior knowledge of the grey levels, the discrete algebraic reconstruction technique (DART) is able to reconstruct objects accurately with projections in a limited angle range. However, the quality of the reconstructions declines as the number of grey levels increases. In this paper, a modified DART (MDART) was proposed, in which each independent region of homogeneous material was chosen as a research object, instead of the grey values. The grey values of each discrete region were estimated according to the solution of the linear projection equations. The iterative process of boundary pixels updating and correcting the grey values of each region was executed alternately. Simulation experiments of binary phantoms as well as multiple grey phantoms show that MDART is capable of achieving high-quality reconstructions with projections in a limited angle range. The interesting advancement of MDART is that neither prior knowledge of the grey values nor the number of grey levels is necessary.

1. Introduction

Tomography techniques have been widely adopted for obtaining three-dimensional images of physical objects non-invasively. Fourier-based methods and algebraic reconstruction methods are two popular types of principal algorithms for image reconstruction. Fourier-based methods, which are directly related to the Radon transform, are still commonly used because of their small computational burden (Mueller *et al.*, 1999). Algebraic reconstruction methods, which formulate the reconstruction problem as a linear system of equations (Zeng, 2010; Herman, 2009), can achieve images with better quality than Fourier-based methods, especially when the number of projections is limited or the angles are in a limited range.

A limited range of tilt angle occurs frequently in electron tomography (Milne & Subramaniam, 2009), soft and hard X-ray nano-tomography (Duke *et al.*, 2013; Tian *et al.*, 2008). A flat sample holder occludes the light when the tilt angle of the tomography reaches a high angle (usually ±75°). The limited spacing for specimen holders between the pole pieces of the objective lens may also prevent the rotation of the sample holders. These would lead to a 'missing wedge' in the collected data. In this case it is very difficult to obtain a quantitative measure of the object based on the reconstruction. In other words, the boundaries and the grey values of the reconstructions do not match well with the physical objects.

Discrete tomography has evolved into a powerful, robust and flexible method for reconstructing images with a small number of projections when the physical objects contain only a few discrete grey levels (Herman & Kuba, 2007). Numerous discrete tomography reconstruction algorithms have been proposed in the last few decades. Schüle *et al.* presented a primal-dual subgradient algorithm for reconstructing binary images from projections with few-view or a limited range of angles (Weber *et al.*, 2004; Schüle *et al.*, 2005). There are many evolutionary algorithms for discrete tomography (Batenburg, 2005; Weber *et al.*, 2006). However, most of these algorithms are limited in achieving a high-quality reconstruction of binary images.

Recently, Batenburg *et al.* proposed the discrete algebraic reconstruction algorithm (DART), which can address binary images and images that contain three or more grey levels with prior knowledge of the grey levels of each material (Batenburg & Sijbers, 2007, 2011; Batenburg *et al.*, 2010). When samples consist of a few discrete materials, it is possible to obtain accurate reconstructions even if the number of projections is limited. Furthermore, thresholding is already applied during the reconstruction, thus DART can achieve segmented images directly. DART has been steadily developed into a powerful algorithm for many experimental datasets, such as reconstructing catalyst particles for bamboo-like carbon nanotubes from transmission electron microscopy (Bals *et al.*, 2007), quantitative analysis of zeolite through discrete electron tomography (Bals *et al.*, 2009) and reconstruction of a diamond from a series of micro-computed tomography projections (Batenburg & Sijbers, 2011).

A common assumption of DART is that all of the grey levels of the reconstruction are known *a priori*; therefore, it is important to know the appropriate assumption of the grey levels and the thresholds for obtaining high-quality reconstructions. Although it is easy to know the grey levels in simulation experiments, obtaining *a priori* knowledge in practice is difficult. To reduce the requirements of prior knowledge, a semi-automatic discrete grey level selection (DGLS) method was proposed to estimate the grey levels of an image (Batenburg *et al.*, 2011). A homogeneous area in the reconstruction is selected manually to calculate the grey value of each grey level. Afterwards, a projection distance minimization DART (PDM-DART) method was proposed to estimate the grey level parameters adaptively; the method required that only the number of grey levels should be known in advance (van Aarle *et al.*, 2012). Some algorithms keep a specific component of the reconstruction fixed, and the rest of the components changed during the process. For example, the BgART algorithm could detect the background and keep the background value fixed for every iteration (Messaoudi *et al.*, 2013). This algorithm facilitates segmentation of objects and denoising of the reconstruction.

The series of algorithms of DART are effective when the number of grey levels is small (Batenburg & Sijbers, 2011). In some actual applications, such as for integrated circuit chips, marine sediment and shale, which have multiple phases and various compositions (Kanitpanyacharoen *et al.*, 2013;

Uramoto *et al.*, 2014), prior knowledge of grey levels, even simply the number of grey levels, is not easy to acquire. As the number of grey levels increases, the reconstruction quality decreases (van Aarle *et al.*, 2012). Hence, it is necessary to develop a method of reconstructing multiple grey images when the range of the tilt angle is limited and without prior knowledge of the grey levels.

In this paper a modified DART (MDART) algorithm is proposed to reconstruct multiple grey images. In our method the available projection data were reconstructed using an algebraic reconstruction method. Then, the reconstruction images were divided into discrete regions depending on threshold values that were selected manually. The segmentation images were used as an input of the proposed method. Each independent region was a research object. The grey values of each discrete region were estimated by solving the algebraic reconstruction linear equations. Thus, the number of unknown variables in the equations was decreased by several orders of magnitude. Then, updating boundary pixels and correcting the grey values of each region were iteratively alternated until the stop criterion or the maximum iteration number was met. This method has been tested on both binary and multiple grey images while the angle of projection was limited.

2. Notation and concepts

Let $\mathbf{x} = (x_j) \in \mathbb{R}^n$ represent a two-dimensional unknown image, which denotes the object function with n pixels. A finite set of m measured projection data $\mathbf{p} = (p_i) \in \mathbb{R}^m$ is defined by

$$\sum_{j=1}^{n} w_{ij} x_j = p_i, \qquad i = 1, 2, \ldots, m, \tag{1}$$

where w_{ij} can be interpreted as the contribution of the jth pixel x_j to the ith detector value p_i. $\mathbf{W} = (w_{ij}) \in \mathbb{R}^{m \times n}$ is the system matrix. Therefore, the tomography reconstruction algorithm tries to find the unknown image $\mathbf{x}$ by solving the linear system of equations

$$\mathbf{W}\mathbf{x} = \mathbf{p}. \tag{2}$$

In practice, numerous reconstruction algorithms have been proposed to solve equation (2) (Kak & Slaney, 2001; Zeng, 2010). For the experiments in this paper, the simultaneous algebraic reconstruction technique (SART) (Andersen & Kak, 1984) TVM (SART-TVM) will be used to reconstruct the images to obtain a preliminary result, and SART will also play an important role in MDART. Therefore, SART and TVM are briefly reviewed. SART is a linear algorithm that finds a solution $\mathbf{x}$ such that the difference between the projections from the original image and the reconstruction image $||\mathbf{W}\mathbf{x} - \mathbf{p}||$ is minimal. Almost all iteration algorithms start with an initial guess $\mathbf{x} = \mathbf{x}^{(0)}$, and a new reconstruction $\mathbf{x}^{(k)}$ is iteratively calculated from $\mathbf{x}^{(k-1)}$. SART carries out updating operations using all projections at an angle each time as follows,

$$x_j^{(k)} = x_j^{(k-1)} + \lambda \frac{1}{\sum_{i=1}^{h} w_{ij}} \sum_{i=1}^{h} \frac{w_{ij}\left(p_i - \sum_{t=1}^{n} w_{it} x_t^{(k-1)}\right)}{\sum_{t=1}^{n} w_{it}}, \quad (3)$$

for $j = 1 \ldots n$, where λ is a relaxation parameter and h is the number of total detectors at each angle.

TVM-based algorithms find the approximate solution as the following optimization problem (Yang *et al.*, 2015),

$$x^* = \arg\min_{x}\left[||Wx - p||_2^2 + \gamma \text{TV}(x)\right], \quad (4)$$

where γ is a regularization parameter indicating the importance of the two terms in the equation and $\text{TV}(\ldots)$ represents the TVM norm, which is the l_1-norm of the gradient image as defined by Sidky *et al.* (2006):

$$\text{TV}(x) = \sum_{i,j,k}\left\{[x(i+1,j,k) - x(i,j,k)]^2\right.$$
$$+ [x(i,j+1,k) - x(i,j,k)]^2$$
$$\left. + [x(i,j,k+1) - x(i,j,k)]^2\right\}^{1/2}. \quad (5)$$

3. The modified discrete algebraic reconstruction technique

The main limitations in traditional discrete tomography methods are the requirements of prior knowledge of the greyscales and the limitation in the number of discrete greyscales. In order to overcome these limitations the MDART algorithm was proposed for reconstruction of incomplete tomographic data of multiple discrete greyscale phantoms without any prior knowledge. A flow chart of the algorithm is shown in Fig. 1. In this approach, we first perform tomographic reconstruction using a traditional algorithm (SART-TVM) to provide an initial guess for further calculation. The initial slice is then segmented based on the greyscales of the image resulting in a number of isolated regions. Since the tomographic data were incomplete, the boundary and the greyscales in all of the regions might not be accurate and need to be improved through iterations. These regions were treated as research objects and their original greyscales disregarded. We then perform a forward Radon transform of the slice with unknown greyscales in all of the regions. The result of the forward Radon transform needs to match the experimentally measured projection data, which enables us to recover the greyscales in the regions by solving the linear equations $\mathbf{W}\mathbf{x}_s = \mathbf{p}$ using the LSRQ method (Paige & Saunders, 1982; Barrett *et al.*, 1994). Due to the uncertainty of the region boundaries, the greyscales on the boundary pixels are further updated by evaluating the difference between the experimentally measured projection data and the Radon transform of the slice with the boundary pixels set to zero. The boundary pixels were smoothed to regularize the boundary reconstruction. The updated intensity in each boundary pixel is used to identify the neighbouring region that has the closest greyscale. This boundary pixel is subsequently merged into the chosen
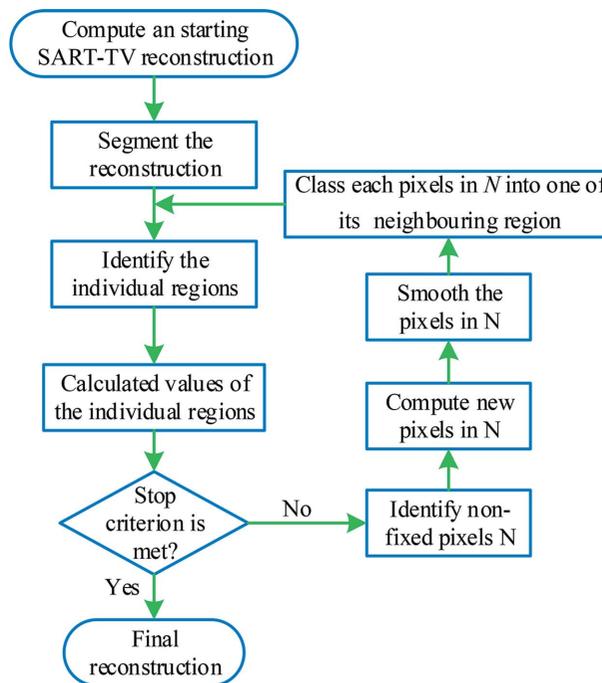

Figure 1
Flow chart of the MDART algorithm.

region, effectively shifting the region boundaries. The above-described procedure is performed iteratively until the stop criterion is met, indicating successful reconstruction of the slice.

There are some main differences with the previous methods. The procedure for identifying regions is added to the algorithm. Each independent region is chosen as a research object, instead of the greyscale. The greyscale of each region was calculated by solving the linear equations. Then the boundary pixel is merged into one of its neighbouring regions that has the closest greyscale.

A simple example is presented to demonstrate the process and details of the algorithm. Fig. 2 indicates the various steps of the algorithm. Fig. 2(*a*) is a binary image with two grey levels (only 0 and 1). Suppose that there were only 121 projections that were equally distributed between $0°$ and $120°$. Fig. 2(*b*) shows the initial guess through SART-TVM reconstruction after 100 iterations. It is obvious that the grey values and the shape of the reconstruction do not match well with the original phantom.

Then, the initial reconstruction was segmented into discrete regions depending on the grey values. Many pieces of software (such as *Amira*, *ImageJ*) could be used to segment the reconstruction with friendly interactive interfaces. To make segmentation work more efficiently, a group of threshold values was chosen to ensure that homogeneous adjacent pixels were divided into the same region as much as possible. For a group of three-dimensional data, a few slices that contain the most compositions are adopted to choose the threshold values. The threshold values should be appropriate for all of the slices. There is no strict requirement for the selection of the threshold, but it would affect the convergence rate of the
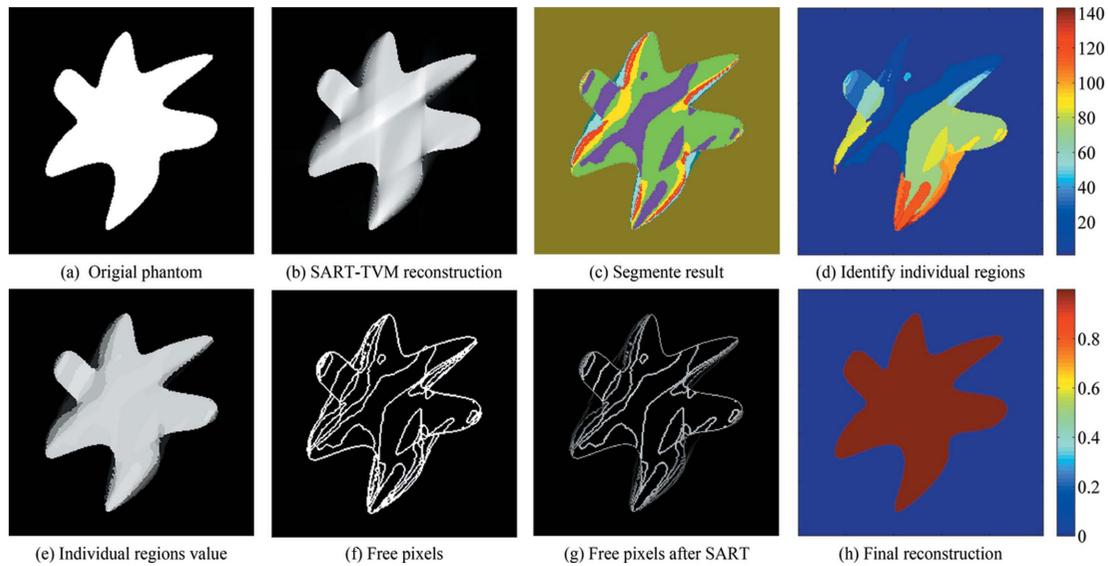
Figure 2
Sequence of operations of the various steps of the MDART algorithm.

algorithm. The threshold values $\tau = (\tau_1 \ldots \tau_l)$ were selected depending on the manual selection. Then, the initial reconstruction was segmented according to the threshold function,

$$s(x_i) = \begin{cases} 1 & (x_i \leq \tau_1) \\ 2 & (\tau_1 < x_i \leq \tau_2) \\ \vdots & \vdots \\ l & (\tau_{l-1} < x_i \leq \tau_l) \\ l+1 & (x_i > \tau_l) \end{cases} . \qquad (6)$$

A group of threshold values $\tau = (225, 200, 165, 70, 20, 10)/255$ is chosen depending on the features of Fig. 2(b). The segmentation result is shown in Fig. 2(c).

The procedure for identifying regions was performed afterwards. If the difference between two adjacent regions was less than the threshold value ε, the two regions were combined. 143 regions are identified and presented in Fig. 2(d).

In this algorithm, each independent region was chosen as a research object, instead of the grey values. Thus, there were 143 unknown variables in the new matrix $\mathbf{x}_s$. The values of each independent region were calculated by solving the linear equations $\mathbf{W}\mathbf{x}_s = \mathbf{p}$ using the LSQR method (Paige & Saunders, 1982; Barrett et al., 1994). The image endowed with new values is shown in Fig. 2(e).

The boundary region N of the image was the set of all pixels that had at least one different pixel in their eight-connected neighbourhoods. The boundary of the image with the new values is shown in Fig. 2(f). Subsequently, the values of the pixels were updated by the SART iterations, while the other pixels were fixed. Thus, the number of variables in the linear equations was obviously reduced compared with the conventional SART. Fig. 2(g) shows the result of the boundary reconstruction after ten SART iterations. To regularize the boundary reconstruction, smoothing must be applied to the boundary pixels. Let b denote the average of eight-connected neighbourhoods of a pixel. The boundary pixels were smoothed with b as follows,

$$x_i^{(t)} = 0.7x_i^{(t)} + 0.3b. \qquad (7)$$

After that, the pixels in N were merged into one of their neighbouring regions that had the closest greyscale.

Subsequently, iterations of the algorithm were performed until the stop criterion was met. In this study, the sum of the squared difference between two successive iteration results was used as a measurement of the degree of convergence. The iterations were stopped once this parameter was smaller than 500 or the maximum iteration number was met.

The final reconstruction of the phantom is shown in Fig. 2(h). It was almost the same as the original phantom image, except for a few pixels with different values. It reveals that MDART is effective while the angle range of the projections is limited.

4. Experiments and discussion

In this section, a series of experiments are presented to demonstrate the reconstruction performance of the proposed method and compared with some commonly used methods. For all algorithms, the six phantom images shown in Fig. 3 were used. Phantom 1 and phantom 2 are binary images (Batenburg & Sijbers, 2011). Phantom 3 and phantom 6 are multiple grey phantoms that contain 15 and 14 grey levels, respectively. Their grey-level distribution is shown in Figs. 3(d) and 3(h), respectively. Phantom 4 is the well known Shepp–Logan phantom, which contains six grey levels. Phantom 5 is composed of 49 homogeneous discs. Every circle has a different value, and a total of 50 grey levels are contained in the phantom. The size of all of the phantoms is 256×256 pixels.

Five reconstruction algorithms were compared in this section. We provide a brief review of them as follows:

(i) FBP. Filtered back projection (FBP) is a Fourier-based method that is related to the inverse Radon transform. In the
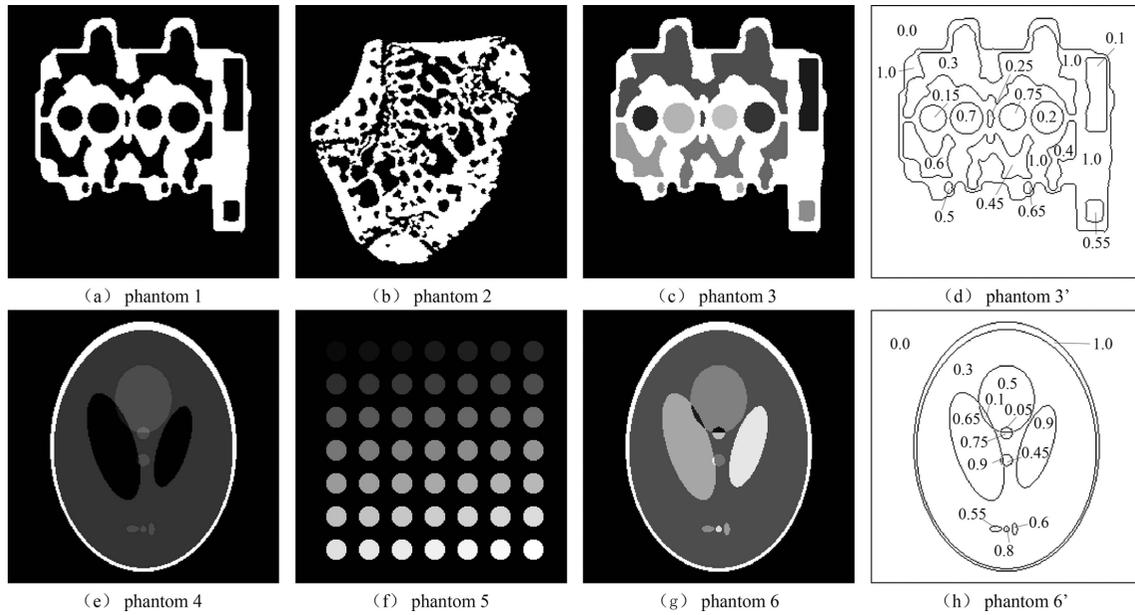
Figure 3
Simulated phantoms used for the simulation experiments: (*a*), (*b*) are binary phantoms; (*c*) is a multiple grey phantom, and its grey values are shown in (*d*); (*e*) Shepp–Logan phantom; (*f*) multiple grey circle phantom; (*g*) multiple grey Shepp–Logan phantom, and (*h*) shows the grey values.

experiments, we used a Ram-Lak filter and linear interpolation in the projection domain as the MATLAB defaults.

(ii) SART. The SART algorithm, which has been described in §2, was run with 500 iterations in the experiments. A positivity constraint was used after each iteration to obtain a better result.

(iii) SART-TVM. This algorithm had also been described in §2, and there are many studies that present details of the algorithm (Sidky *et al.*, 2006; Yu & Wang, 2009; Liang *et al.*, 2013). In this work, we refer to the original article (Sidky *et al.*, 2006) for details except using SART to replace ART. We used $a = 0.2$ (gradient descent parameter), $N_{grad} = 20$ (the total number of gradient descent steps) and 500 iterations for the analysis.

(iv) DART. The DART algorithm program is included in the *ASTRA* toolbox (Palenstijn *et al.*, 2013) and is available online. 500 iterations were performed to obtain convergent reconstructions. The grey levels and threshold values were applied as prior knowledge, but they were not adopted in the four other algorithms. The 500 SIRT algebraic reconstruction method has been used for the initial reconstruction and 15 in the successive ones. The fix probability is 0.99, and equation (7) is used to smooth the boundary reconstruction.

(v) MDART. Details of MDART were described in §3. The threshold value ε of the regions that need to be identified was 0.01 in the experiments.

The total number of different pixels between the reconstruction and original image was used as the performance metric. Because prior knowledge of the grey levels was not used in all of the algorithms, except for DART, the segmentation process was not performed after the iteration step. Therefore, a certain degree of difference in the pixel values between the reconstruction and original image was acceptable.

We define the computing method for the total number of different pixels as follows:

$$K = \left| \left\{ i \left| \left[\left| x_i^r - x_i \right| \, > \, \max(\omega \Delta \rho, 0.003) \right] \right\} \right| \right|, \quad (8)$$

where $\Delta \rho$ is the minimum interval between the two grey levels in the original images; ω is an indicator between 0 and 1 ($\omega = 0.03$ was used in the experiment); and $\omega \Delta \rho$ is the threshold value of the errors. However, ordinary image formats are usually 256 grey levels. When the difference of a pixel between the reconstruction and original image is less than a grey level it can be ignored. Thus, when $\omega \Delta \rho < 0.003$, the threshold is set to 0.003.

If prior knowledge of the grey levels $\boldsymbol{\rho} = (\rho_1, \rho_2, \ldots, \rho_l)$ is known in advance, the reconstructions can be segmented as follows:

$$s(x_i) = \begin{cases} \rho_1, & x_i \leq (\rho_1 + \rho_2)/2 \\ \vdots & \\ \rho_i, & (\rho_{i-1} + \rho_i)/2 < x_i \leq (\rho_i + \rho_{i+1})/2 \\ \vdots & \\ \rho_l, & x_i > (\rho_{l-1} + \rho_l)/2 \end{cases} \quad (9)$$

The relative error of the value of the grey levels was defined as follows:

$$\frac{\left| \rho_i^r - \rho_i \right|}{\max(\{\rho_i\})} \times 100\%, \quad i = 1 \ldots l. \quad (10)$$

4.1. Binary phantoms reconstruction

In this section, we present the reconstruction results of binary phantoms based on the projections with a limited
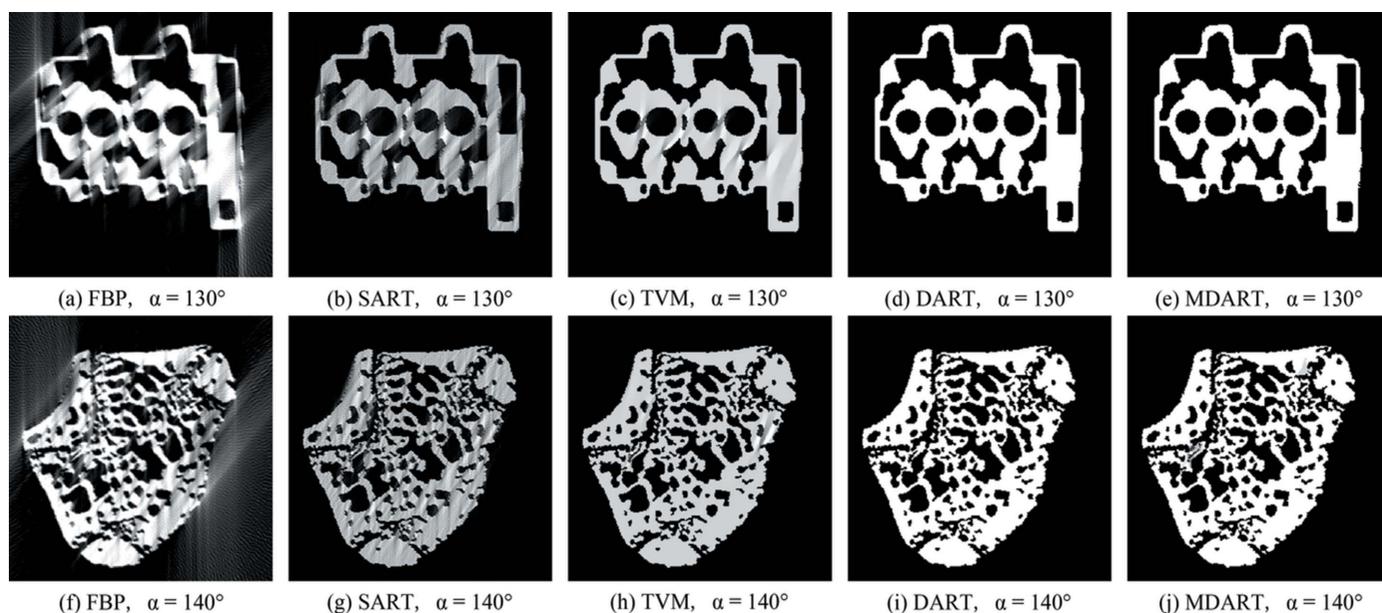
Figure 4
Reconstructions of binary images using FBP (column 1), SART (column 2), TVM (column 3), DART (column 4) and MDART (column 5). Phantom 1 has an angular range of $\alpha = 130°$ and phantom 2 has an angular range of $\alpha = 140°$.

angular range. As mentioned above, for the DART algorithm, prior knowledge of the grey levels is necessary, whereas, for other techniques, it is not required. Fig. 4 shows the reconstructions of phantom 1 with an angle range of 130° and phantom 2 with an angle range of 140° by FBP, SART, TVM, DART and MDART. The angular step is 1°. Obviously, when the angular range of the projections is limited, a missing wedge has a significant influence on the reconstructions using FBP and SART. The pixel error distribution caused by using five algorithms as a function of the angular range is shown in Fig. 5, and the total number of all the phantoms is 65536. The results of TVM, DART and MDART are more accurate as the angle range increases. Combining Figs. 4 and 5, the reconstruction of MDART is better than TVM for the same projections. If prior knowledge of the grey level is applied, DART can obtain very

accurate reconstructions of the binary phantoms with a small angle range. It can be concluded that, for binary images of a limited angle range, MDART can achieve high-quality reconstructions without prior knowledge of the grey levels.

4.2. Multiple grey phantoms reconstruction

For most discrete tomography reconstruction algorithms, it is a challenge to reconstruct a multiple-level grey image. Conventional continuous reconstruction methods cannot achieve high-quality results when the angle range is limited because of the 'missing wedge' of data. Fig. 6 shows the reconstructed results of phantoms 3, 4, 5 and 6 using the five methods. Many artifacts and deformations of morphology could be 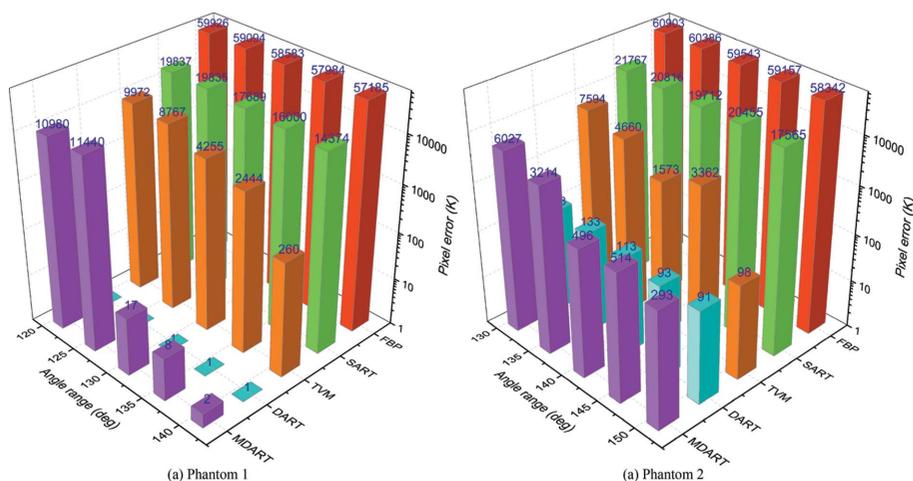found in the reconstructions of FBP and SART. The results of TVM showed a very undesirable staircase effect as the number of grey levels increases. DART also suffered from the missing wedge influence. The MDART technique showed good behaviour for both morphology and grey value. The pixel error K as a function of the angle range of the projections for FBP, SART, TVM, DART and MDART is shown in Fig. 7, where erroneous pixels number are calculated using equation (8). The angular step in all cases is 1° between the projections. It clearly showed that, even without using prior knowledge of the grey levels, MDART performs better than FBP, SART, TVM and DART when processing multiple grey phantoms in a limited angle range.

Figure 5
Pixel error K as a function of the angle range of the projections for FBP, SART, TVM, DART and MDART.

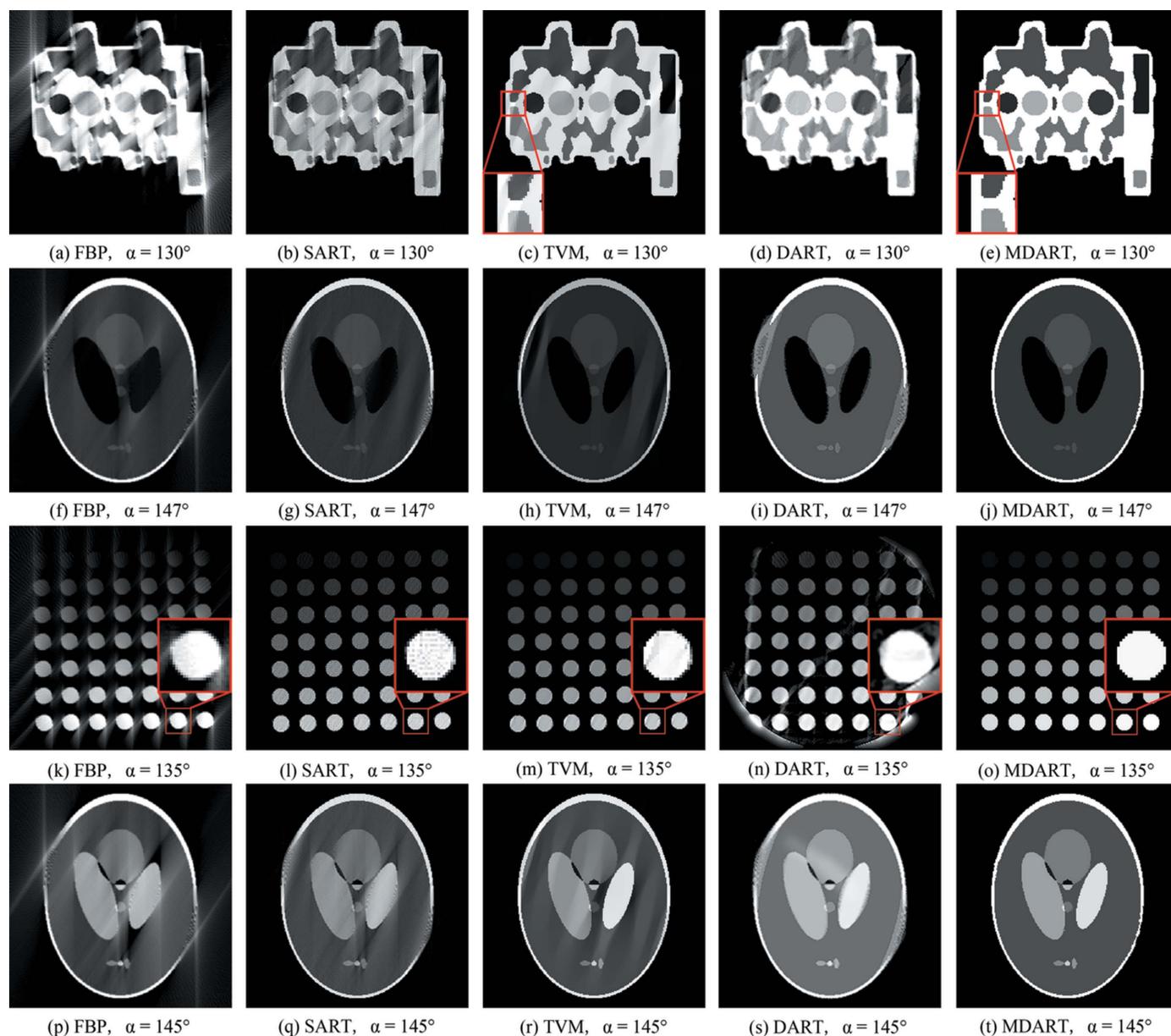Zhiting Liang *et al.* • Multiple grey image reconstruction **611**

Figure 6
Reconstructions of multiple grey phantoms using FBP (column 1), SART (column 2), TVM (column 3), DART (column 4) and MDART (column 5). Phantom 3 has an angular range of $\alpha = 130°$, phantom 4 has an angular range of $\alpha = 147°$, phantom 5 has an angular range of $\alpha = 135°$ and phantom 6 has an angular range of $\alpha = 145°$.

Fig. 8 shows the number of error pixels of the reconstructions that have been segmented by equation (9) as a function of the angle range of the projections. When the results obtained by FBP, SART and TVM have been segmented, all of the reconstructed results obviously improved. However, it was obvious that the number of error pixels of MDART was still much less than for the four other methods. Note that segmentation was not applied to the reconstructions of DART because they had already been segmented in the algorithm.

The limitation of the number of grey levels was also investigated. Phantoms, resembling phantom 5, were tested with an increasing number of discs and grey levels. For each phantom, varying angle ranges of projections were simulated. The pixel error K of the reconstructed images as a function of the angle range is shown in Fig. 9. As the number of grey levels increased, the quality of the reconstructions decreased.

The relative errors of the grey value of phantoms 3, 4, 5 and 6 using MDART were calculated using equation (10) in a different angle range, as shown in Fig. 10. For the four multiple grey phantoms, the relative errors decreased to a low level with the angle range increased. Most of the relative errors are less than 1% when, for the angle range of phantom 3, $\alpha > 135°$; for phantom 4, $\alpha > 137°$; for phantom 5, $\alpha > 120°$; and for phantom 6, $\alpha > 150°$. The precision is good enough to distinguish different compositions. It shows that, for most of the phantoms, an angle range of 150° can usually result in a precise reconstruction. MDART is suitable for multiple grey phantom reconstruction in a limited angle range.
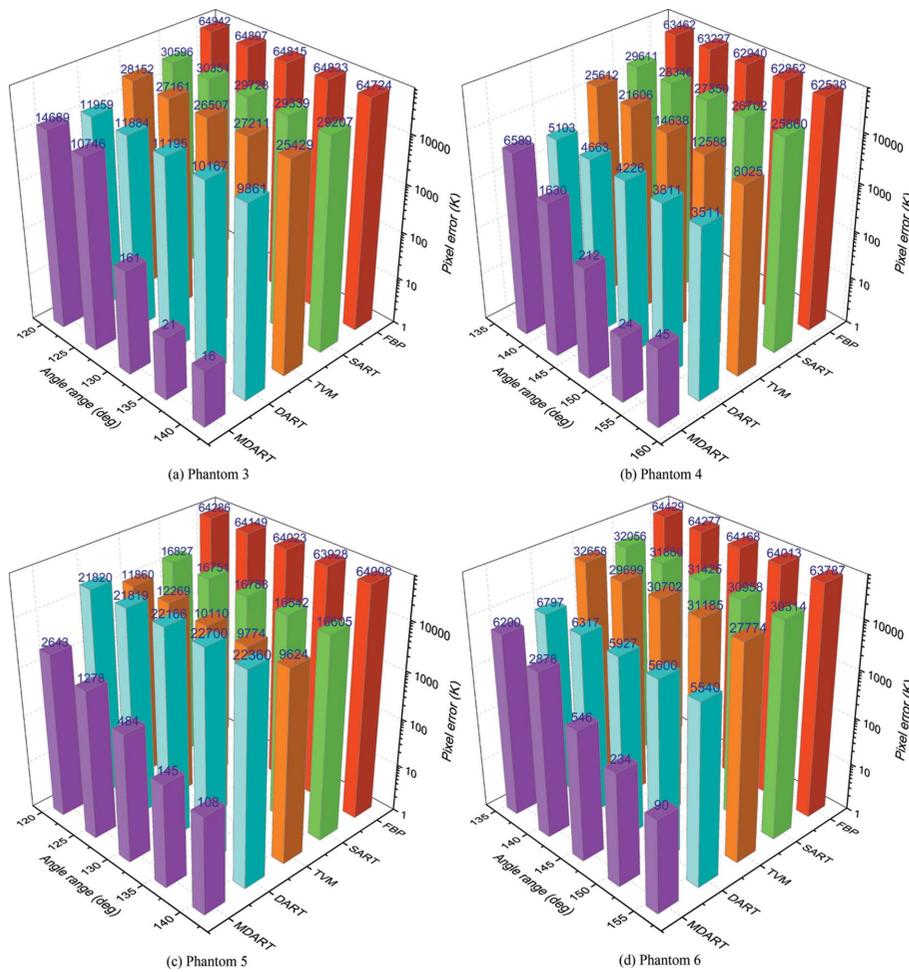
Figure 7
Pixel error K as a function of the angle range of the projections for FBP, SART, TVM, DART and MDART.

4.3. Convergence

To understand the impact of the initial value of the segmentation on the algorithm, a multiple grey image, phantom 3, with an angle range of $130°$ is tested.

To segment the reconstruction of the SART-TV result into discrete regions, a group of threshold values was chosen. In Table 1 there are ten groups of threshold values with different values. The threshold values of the first eight groups are chosen depending on the features of the reconstruction. The ninth group, which is roughly segmented, is a case where the third hole in the figure is not identified, as shown in Fig. 11(d). The tenth group starts with a hole in the middle that spreads outward. The eleventh group is segmented without threshold values, but it is manually marked with some obvious feature regions, as shown in Fig. 11(f). Some of the segmentation results are shown in Figs. 11(b)–11(e), and the others are shown in Figs. S1 and S2 of the supporting information. Using different segmentation results as an input to MDART leads to a different number of required iterations and different final error, as shown in Table 1. The values of the error pixels are slightly different. The number of error pixels as a function

of the iteration number is shown in Fig. 11(g). The threshold values are related to the convergence rate of the algorithm. For three-dimensional data, a few typical slices are used to select the threshold values, and then the threshold values are applied to the entire three-dimensional data. Overall, the method of selecting the threshold values using software (such as *Amira*, *ImageJ*, *etc.*) is convenient and robust.

In the past decade, many important tomography reconstruction methods have been proposed. Equally sloped tomography with oversampling reconstruction (Miao *et al.*, 2005) overcomes the limitation of interpolation error of the points from a polar grid to a Cartesian grid in Fourier space. This method has been applied to many tomography fields. Liu *et al.* proposed an iterative algorithm to reconstruct the refractive index information from data collected by an analyzer-based imaging setup (Liu *et al.*, 2007). It is effective and accurate compared with the standard analytical method. For discrete tomography, several competing algorithms also have been presented. DART has proved to be a successful algorithm for objects consisting of only a few different compositions with prior knowledge of the grey levels (Batenburg & Sijbers, 2011). PDM-DART has been applied in tomography that requires prior knowledge only of the number of grey levels (van Aarle *et al.*, 2012). A partially discrete algebraic reconstruction technique (PDART) could reconstruct and segment the densest nanoparticles and allow the rest of the reconstruction to vary freely (Roelandts *et al.*, 2011). The BgART algorithm detects the background and keeps the background fixed at a uniform value for every iteration (Messaoudi *et al.*, 2013). This facilitates denoising the reconstruction and segmentation of objects without prior knowledge of the materials. The MDART algorithm treats each region as a research object, and the value of each region is calculated by solving the linear system of equations. It reconstructs images with multiple compositions without prior knowledge of the grey values.

5. Conclusions

In this paper, a modified DART (MDART) algorithm for reconstructing an image with multiple grey and discrete regions is presented. MDART focuses on reconstructing images with a limited angle range and without prior knowledge of the grey values. By using each independent region instead of pixels as a research object, the number of unknowns
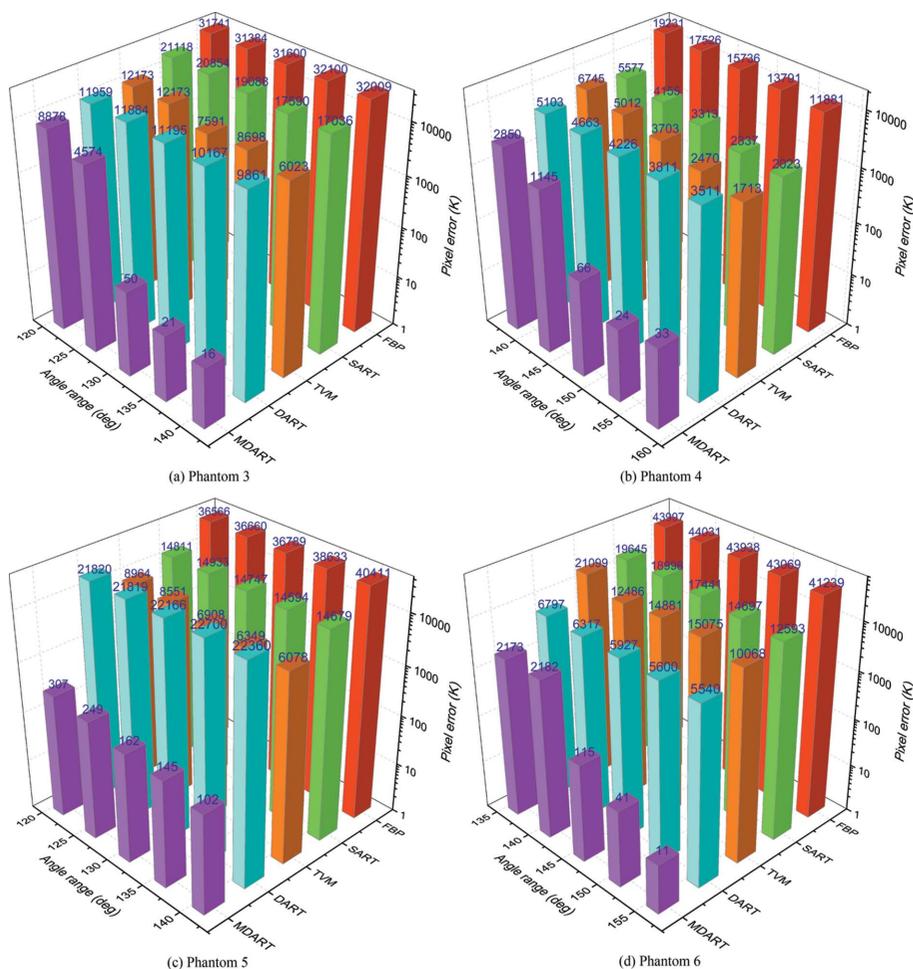
Figure 8
Pixel error *K* as a function of the angle range of the projections for FBP, SART, TVM, DART and MDART. The results have been segmented with prior knowledge of the grey levels.

a major challenge for quantitative analysis of an object when using tomography methods. MDART can achieve a higher-quality reconstruction without prior knowledge of the grey levels for both binary and multiple grey phantoms. The number of erroneous pixels in the multiple grey reconstructions using MDART is smaller than the numbers obtained by other reconstructed methods. Although the number of grey levels increases to 50, there is no obvious reduction in the accuracy. Additionally, the grey level values calculated using MDART are precise enough when compared with the original images. Thus, MDART can be used as an alternative method to quantitatively analyze objects with multiple compositions, such as integrated circuit chips, the cathode and anode of a solid oxide fuel cell, marine sediment, shale, nanoparticles, *etc*. In future work, we intend to optimize the algorithm to make it suitable for different types of experimental data with discrete compositions obtained from soft X-ray microscopy, hard X-ray microscopy, electron microscopy, *etc*.

in the algebraic reconstruction linear equations is decreased by several orders of magnitude.

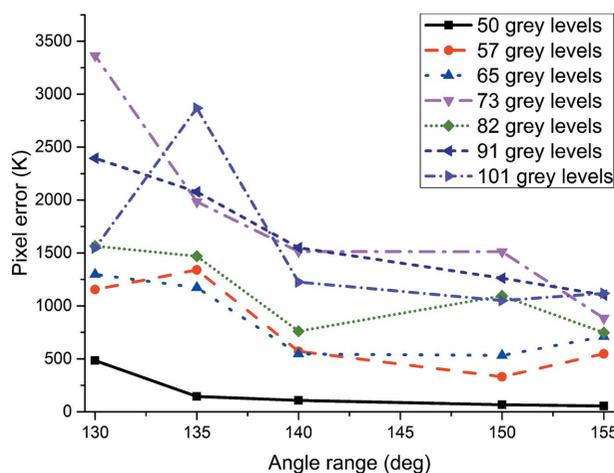The results show that MDART is a powerful algorithm for compensating for the 'missing wedge' effects that present

Figure 9
Pixel error *K* of the reconstructed images as a function of the angle range of the projections for seven phantoms with different numbers of grey levels; the total number of pixels in the phantoms is 65536.

References

Aarle, W. van, Batenburg, K. J. & Sijbers, J. (2012). *IEEE Trans. Image Process.* **21**, 4608–4621.

Andersen, A. & Kak, A. (1984). *Ultrason. Imaging*, **6**, 81–94.

Bals, S., Batenburg, K. J., Liang, D. D., Lebedev, O., Van Tendeloo, G., Aerts, A., Martens, J. A. & Kirschhock, C. E. A. (2009). *J. Am. Chem. Soc.* **131**, 4769–4773.

Bals, S., Batenburg, K. J., Verbeeck, J., Sijbers, J. & Van Tendeloo, G. (2007). *Nano Lett.* **7**, 3669–3674.

Barrett, R., Berry, M. W., Chan, T. F., Demmel, J., Donato, J., Dongarra, J., Eijkhout, V., Pozo, R., Romine, C. & Van der Vorst, H. (1994). *Templates for the Solution of Linear Systems: Building Blocks for Iterative Methods.* Philadelphia: Siam.

Batenburg, K. J. (2005). *Discrete Appl. Math.* **151**, 36–54.

Batenburg, K. & Sijbers, J. (2007). *IEEE International Conference on Image Processing (ICIP 2007)*, pp. IV-133–IV-136. IEEE.

Batenburg, K. J. & Sijbers, J. (2011). *IEEE Trans. Image Process.* **20**, 2542–2553.

Table 1
The algorithm progress of ten groups of threshold values; manual segmentation is used to segment the SART-TV reconstruction.

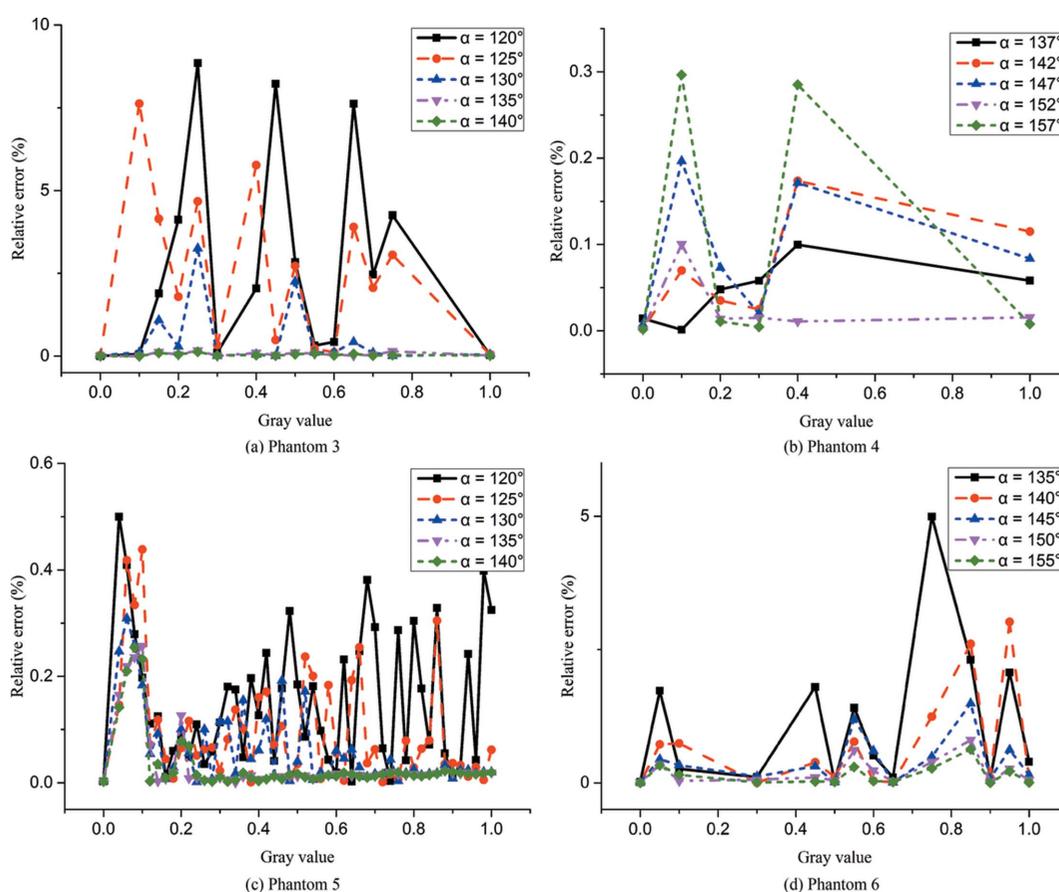|	Segment number										
	1	2	3	4	5	6	7	8	9	10	11
Threshold values (/255)	240	235	230	220	225	230	195	190	178	240	
	225	220	215	195	180	200	135	50	130	230	
	205	195	185	155	150	160	70	10	90	215	
	185	160	155	125	120	120	40		55	175	
	160	140	130	85	85	80	10		10	125	
	135	120	100	60	60	35				65	
	115	90	65	35	30	9				45	
	90	60	35	10	10					25	
	65	35	10							10	
	30	10									
	10										
Pixel error	201	223	603	149	152	642	596	144	597	155	446
Iterations	40	73	38	99	59	41	26	6	110	344	220

Figure 10
Relative error of the grey value of the MDART reconstructions of phantoms 3, 4, 5 and 6 in different angle range.

Batenburg, K. J., Sijbers, J., Poulsen, H. F. & Knudsen, E. (2010). *J. Appl. Cryst.* **43**, 1464–1473.
Batenburg, K. J., van Aarle, W. & Sijbers, J. (2011). *Pattern Recognit. Lett.* **32**, 1395–1405.
Duke, E. M., Razi, M., Weston, A., Guttmann, P., Werner, S., Henzler, K., Schneider, G., Tooze, S. A. & Collinson, L. M. (2013). *Ultramicroscopy*, **143**, 77–87.
Herman, G. T. (2009). *Fundamentals of Computerized Tomography: Image Reconstruction from Projections.* Springer.
Herman, G. T. & Kuba, A. (2007). *Advances in Discrete Tomography and its Applications.* Berlin: Springer.

Kak, A. C. & Slaney, M. (2001). *Principles of Computerized Tomographic Imaging.* Philadelphia: Society for Industrial and Applied Mathematics.
Kanitpanyacharoen, W., Parkinson, D. Y., De Carlo, F., Marone, F., Stampanoni, M., Mokso, R., MacDowell, A. & Wenk, H.-R. (2013). *J. Synchrotron Rad.* **20**, 172–180.
Liang, Z., Guan, Y., Liu, G., Bian, R., Zhang, X., Xiong, Y. & Tian, Y. (2013). *Proc. SPIE*, **8851**, 885113.
Liu, Y. J., Zhu, P. P., Chen, B., Wang, J. Y., Yuan, Q. X., Huang, W. X., Shu, H., Li, E. R., Liu, X. S., Zhang, K., Ming, H. & Wu, Z. Y. (2007). *Phys. Med. Biol.* **52**, L5–13.
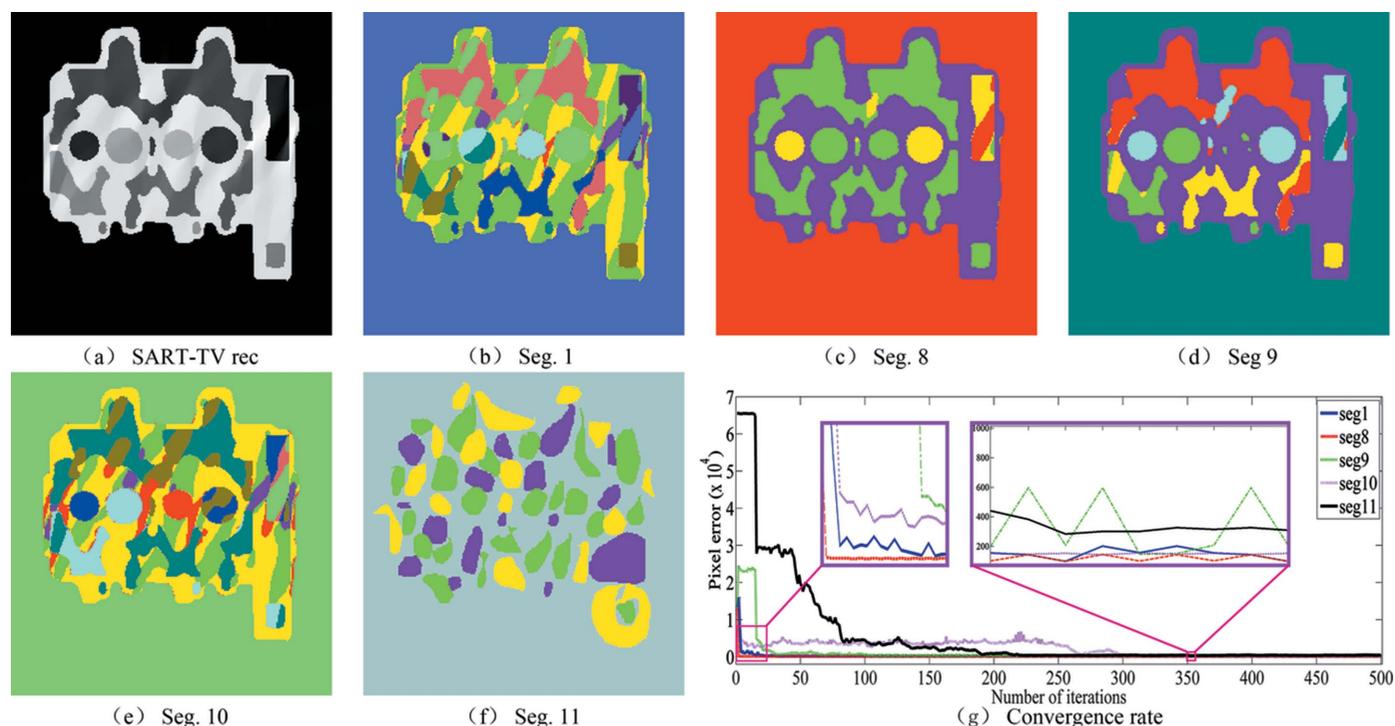
Figure 11
Segment results of the SART-TV reconstruction of phantom 3 and the convergence rate of different segment results. (*a*) The reconstruction of SART-TV with an angular range of $\alpha = 130°$. (*b*) Segmented carefully with 11 threshold values. (*c*) Segmented with three threshold values. (*d*) One of the holes in the middle is not identified. (*d*) One of the holes in the middle spreads outward. (*f*) According to the reconstruction, a few obvious features of the regions are marked out manually. (*g*) The convergence rates of different segment results as an initial input into the MDART.

Messaoudi, C., Aschman, N., Cunha, M., Oikawa, T., Sorzano, C. O. & Marco, S. (2013). *Microsc. Microanal.* **19**, 1669–1677.

Miao, J., Förster, F. & Levi, O. (2005). *Phys. Rev. B*, **72**, 052103.

Milne, J. L. & Subramaniam, S. (2009). *Nat. Rev. Microbiol.* **7**, 666–675.

Mueller, K., Yagel, R. & Wheller, J. J. (1999). *IEEE Trans. Med. Imaging*, **18**, 519–537.

Paige, C. C. & Saunders, M. A. (1982). *ACM Trans. Math. Softw.* **8**, 43–71.

Palenstijn, W. J., Batenburg, K. J. & Sijbers, J. (2013). *The ASTRA Tomography Toolbox*, in *Proceedings of the 13th International Conference on Computational and Mathematical Methods in Science and Engineering (CMMSE 2013)*, 24–27 June 2013, Cabo de Gata, Almeria, Spain.

Roelandts, T., Batenburg, K. J. & Sijbers, J. (2011). *Proceedings of the 11th International Meeting on Fully Three-Dimensional Image Reconstruction in Radiology & Nuclear Medicine (Fully 3D)*, Potsdam, Germany.

Schüle, T., Schnörr, C., Weber, S. & Hornegger, J. (2005). *Discrete Appl. Math.* **151**, 229–243.

Sidky, E. Y., Kao, C.-M. & Pan, X. (2006). *J. X-ray Sci. Technol.* **14**, 119–139.

Tian, Y. C., Li, W. J., Chen, J., Liu, L. H., Liu, G., Tkachuk, A., Tian, J. P., Xiong, Y., Gelb, J., Hsu, G. & Yun, W. B. (2008). *Rev. Sci. Instrum.* **79**, 103708.

Uramoto, G.-I., Morono, Y., Uematsu, K. & Inagaki, F. (2014). *Limnol. Oceanogr. Methods*, **12**, 469–483.

Weber, S., Nagy, A., Schulle, T., Schnorr, C. & Kuba, A. (2006). *Lect. Notes Comput. Sci.* **4245**, 146–156.

Weber, S., Schule, T., Hornegger, J. & Schnorr, C. (2004). *Lect. Notes Comput. Sci.* **3322**, 38–51.

Yang, X., Hofmann, R., Dapp, R., van de Kamp, T., dos Santos Rolo, T., Xiao, X., Moosmann, J., Kashef, J. & Stotzka, R. (2015). *Opt. Express*, **23**, 5368–5387.

Yu, H. & Wang, G. (2009). *Phys. Med. Biol.* **54**, 2791–2805.

Zeng, G. L. (2010). *Medical Image Reconstruction: A Conceptual Tutorial.* Berlin: Springer.